Birkbeck
UNIVERSITY OF LONDON

BIROn - Birkbeck Institutional Research Online

Laug, A. and Schwarz, A. and Lauterbach, S. and Engels, Stefan and Schwalb, A. (2020) Ecosystem shifts at two Mid-Holocene tipping points in the alpine Lake Son Kol (Kyrgyzstan, Central Asia). The Holocene 30 (10), pp. 1410-1419. ISSN 0959-6836.

Downloaded from: https://eprints.bbk.ac.uk/id/eprint/31673/

Usage Guidelines:
Please refer to usage guidelines at https://eprints.bbk.ac.uk/policies.html or alternatively contact lib-eprints@bbk.ac.uk.

Ecosystem Shifts at two Mid-Holocene Tipping Points in the alpine Lake Son Kol (Kyrgyzstan, Central Asia)

Laug, Andreas[1], Schwarz, Anja[1], Lauterbach, Stefan[2], Engels, Stefan[3], Schwalb, Antje[1]

[1] Technische Universität Braunschweig, Institute of Geosystems and Bioindication, Langer Kamp 19c, 38106 Braunschweig, a.laug@tu-bs.de, +495313197274, anja.schwarz@tu-bs.de, antje.schwalb@tu-bs.de,

[2] Christian-Albrechts-Universität zu Kiel, Leibniz-Labor für Altersbestimmung und Isotopenforschung, Max-Eyth-Str. 11-13, D-24118 Kiel, Germany, slauterbach@leibniz.uni-kiel.de

[3] Birkbeck University of London, Department of Geography, 32 Tavistock Sq., London, WC1H 9EZ, UK, s.engels@bbk.ac.uk

Abstract

Tipping points can be defined as critical ecosystem thresholds that start self-enforced dynamics pushing systems into new stable states. Many lake ecosystems of arid Central Asia are sensitive to hydrological changes as they are located at the intersection of the influence of the dry Siberian Anticyclone and the relatively humid mid-latitude Westerlies, and their sediment records can be used to study past tipping points. We studied subfossil chironomid remains preserved in a ca. 6000-year-long sediment record from the Central Asian lake Son Kol (Central Kyrgyzstan) to reconstruct past ecosystem dynamics. Our results show abrupt transitions from a chironomid fauna dominated by macrophyte-associated, salinity-indicating taxa, to a vegetation-independent fauna, and subsequently to a macrophyte-associated, freshwater-indicating fauna. A comparison of the chironomid-based environmental reconstruction to other proxy indicators from the same record suggests a phase of increased Westerly strength starting about 4900 cal. yr BP. This increase led to enhanced precipitation and sediment fluxes into the lake, which in turn led to high turbidity levels and consequently to a macrophyte collapse causing abrupt changes in the chironomid fauna. At 4300 cal. yr BP, a weakening of the Westerlies in combination with higher lake levels led to lower turbidity and ultimately to the recovery of the macrophyte population and associated changes in the chironomid assemblage. These two sequences of events show how the occurrence of a gradual change in an external trigger (Westerlies) can trigger a cascade of within-lake processes (turbidity, macrophyte density) and may ultimately lead to an abrupt reorganisation of the ecosystem (chironomid fauna), providing models for tipping points.

Keywords: Holocene, Chironomids, Westerlies, Paleoecology, Macrophytes

Introduction

Originating in social sciences (Grodzins, 1958), the term “tipping point” has been used in ecological discussions to describe the situation when ecosystem changes reach a threshold from which self-enforcing dynamics lead the system into a new stable state (van Nes et al., 2016). In lakes, these regime shifts are particularly common when climatic or anthropogenic influence causes major hydrological and/or ecological changes (Andersen et al., 2009; Lees et al., 2006; Randsalu-Wendrup et al., 2014, 2016). Understanding tipping point dynamics is of particular interest for the future, because many systems will reach such thresholds under continuing climate change (Lenton et al., 2008). In order to clearly describe the processes around the tipping points, we differentiated between triggers, actors pushing the ecosystem to the threshold, and drivers, actors of the self-enforcing feedback-loop.

Regions characterized by the limitation of an important climatic factor, such as frost-free days or precipitation are particularly sensitive to changes in climate and therefore excellent for investigating tipping points. For many ecosystems in arid Central Asia, changes in precipitation and water availability are of crucial importance. As precipitation is mainly provided by the mid-latitude Westerlies (Aizen et al., 1997, 2001), even minor fluctuations of their interplay with dry air masses from the Siberian High can lead to major differences in the water budget. Therefore, reconstructing ecosystem dynamics of arid Central Asia plays a key role in understanding the dynamics of these two atmospheric circulation systems (Cheng et al., 2012) as well as possible responses of freshwater ecosystems to climate forcing. The central Kyrgyz lake Son Kol is situated in the transition zone between the two wind systems (Aizen et al., 1997, 2001), and therefore provides an excellent opportunity to study their past interactions.

Lake sediments typically contain a range of proxies, such as diatoms, ostracods and chironomids (Alivernini et al., 2018; Battarbee, 2000; Brooks 2006; Schwalb et al. 1998), that can be studied to reconstruct ecosystem development (Beer et al., 2007; Mischke and Wünnemann, 2006; Schwarz et al., 2017). Previous studies from Son Kol reported the development from a saline to a freshwater lake including major hydrological changes caused by moister climate conditions ca. 5000–4500 cal. yr BP (Huang et al., 2014; Lauterbach et al., 2014; Mathis et al., 2014; Pacton et al., 2014; Schwarz et al., 2017). The sediment core examined in this study was first investigated by Lauterbach et al. (2014) using sedimentological, (bio)geochemical, isotopic, and palynological evidence to reconstruct phases of enhanced allochthonous sediment input through snowmelt, reflecting increased winter snowfall brought by episodically intensified Westerlies in Central Kyrgyzstan during the last 6000 years. For the same record, Schwarz et al. (2017) combined diatom, ostracod and stable isotope data derived from the Son Kol sediment record and identified climate-driven organism responses. Both studies showed ecosystem-wide abrupt shifts at ca. 5000 and 4300 cal. yr BP. Diatoms, however, were occasionally poorly or not continuously preserved in the sediment, especially from 4900 to 4300 cal. yr BP, therefore leaving final conclusions about internal processes affecting the ecosystem open.

Subfossil remainsof chironomid larvae (Diptera: Chironomidae) are preserved in lake sediments due to their high chitin concentration. They can be especially valuable where other bioindicators such as diatoms are poorly preserved due to alkaline conditions (Brooks, 2006; Caballero et al., 2003; Flower, 1993). They have been widely used to reconstruct past

environmental conditions, including summer air temperatures (Brooks and Birks, 2000; Zhang et al., 2017), water depth (Engels et al., 2012), salinity (Chen et al., 2009) and pH (Charles et al., 1987: Plank, 2010). Furthermore, the association of different chironomid taxa with specific habitats, such as submerged macrophyte vegetation, can give an insight into ecosystem changes beyond the physicochemical conditions (Motta and Massaferro, 2019).

In this paper, we present the results of detailed chironomid analysis applied to the Holocene record of Son Kol. Combining our new results with existing data on past environmental change at the site (Lauterbach et al., 2014; Schwarz et al., 2017) allows us to study ecosystem dynamics across the past 6000 years. We specifically aim to (1) reveal ecosystem shifts, (2) identify the cascade which generated the observed abrupt shifts, including both triggers and drivers, as well as (3) define tipping points and distinguish them from other changes

Study Site

Son Kol (41° 50' N, 75° 10' E) is the second largest lake of Kyrgyzstan, with a surface area of ca. 273 km^2 (Fig. 1). The relatively shallow lake (max. water depth ca. 13 m) is situated at 3016 m a.s.l. in the central Tian Shan. It is surrounded by mountain ranges peaking at 3800-4000 m a.s.l., forming a ca. 1130 km^2 catchment area (Academy of Science of the Kyrgyz SSR, 1987; Shnitnikov, 1980). Catchment geology is composed of Cambro-Ordovician granitoids, carboniferous sedimentary rocks and Permian granitoids, sedimentary rocks and tuffs. The plains around the lake consist of eroded Quaternary sediments (De Grave et al., 2011). The main water sources are precipitation, snowmelt runoff and groundwater inflow. The lake is drained by one outlet at its eastern end (Lauterbach et al., 2014).

Short temperate summers and long, cold winters with snow cover from November to April characterize the local, high-alpine, continental climate. The average annual temperature is -3.5 °C (average in January -20 °C, in July 10 °C), providing ice cover from October to late April (Academy of Science of the Kyrgyz SSR, 1987; Lauterbach et al., 2014; Schwarz et al., 2017; Shnitnikov, 1980). Due to the shallow water depth and strong winds, Son Kol is polymictic and well oxygenated throughout the year, featuring water temperatures of 0–2 °C in winter and ca. 16 °C in summer (Lauterbach et al., 2014). Today it is a freshwater lake with conductivities ranging between 0.515 and 0.530 mS cm^{-1} (Schwarz et al., 2017).

The Siberian Anticyclone in winter and the mid-latitude Westerlies in summer are the wind systems that control the regional climate. Because the Westerlies are the main water source, the annual precipitation of 500-600 mm is seasonally distributed, with only 20 % falling in winter (Academy of Science of the Kyrgyz SSR, 1987; Aizen et al., 1997, 2001). The Son Kol region is today located north of the monsoon influenced area and likely has been since the mid-Holocene (Cheng et al., 2012; Winkler and Wang, 1993). The vegetation surrounding the lake is characterized by alpine meadows, steppe-desert landscapes (Mathis et al., 2014) as well as sedge marsh at the lake shores, followed by submerged macrophytes, eg *Myriophyllum,* and algae on the lake bottom down to water depths of at least 7–8 m (Lauterbach et al., 2014).

[Insert Fig. 1]

Methods

Two sediment cores of 121.5 cm (SONK_11_D1) and 166.0 cm (SONK_11_D2) length were retrieved in the summer of 2011 from the south-eastern part of Son Kol (41°47‘38‘‘N, 75°11‘49‘‘E, 10.5 m water depth; Fig. 1), using an UWITEC gravity corer. The two sediment cores were correlated using distinct lithological marker layers, resulting in a continuous 173.5 cm long composite sediment record (SONK_11_D1/2; Lauterbach et al., 2014). To establish a chronology for the composite sediment record, 28 samples of terrestrial plant macrofossil remains, bivalve shells, and bulk sediment were dated by accelerator mass spectrometry (AMS) ^{14}C dating at the Poznań Radiocarbon Laboratory. The final age-depth model for the composite sediment core was established by Bayesian age modelling using a *P Sequence* depositional model implemented in OxCal 4.1 (Bronk Ramsey, 2008, 2009). As model input parameters we used 22 of the obtained (AMS ^{14}C dates, which were calibrated with the IntCal09 calibration data set (Reimer et al., 2009), as well as age information from ^{137}Cs and ^{241}Am activity measurements obtained from the uppermost 10 cm of the composite sediment record. According to the final age-depth model, the sediment sequence covers the last 6000 years. A detailed description of the sedimentology of the composite core, as well as comprehensive information about AMS ^{14}C dating and age modelling, is provided by Lauterbach et al. (2014).

In total, 118 samples were analysed for chironomid remains: 32 one-cm-thick samples were collected from core SONK_11_D1 (12-98 cm composite depth); another 86 samples, each 0.5 cm thick, were retrieved from core SONK_11_D2 (99-173.5 cm composite depth). Sample depths are given as middle depth in addition to the core abbreviation 11_D1/11_D2. A minimum of 1 g sediment was analysed, with the exception of one sample (11-D2, 140.5 cm composite depth) that did not provide sufficient sediment. Sample preparation followed Brooks et al. (2007). After solution in 10 % KOH and 20 minutes of heating up to 85 °C, the sediment was rinsed through a 100 µm mesh sieve. Chironomidae head capsules (HC) as well as Cladocera ephippia and Charophyta oogonia were hand-picked at 32 x magnification and mounted in Euparal© mounting medium. Identification under 400 x magnification followed Brooks et al. (2007), Rieradevall and Brooks (2001), and Bitušík and Hamerlík (2014). The water content of samples was determined using freeze drying (two measurements per sample). Dry weights of samples were subsequently used to determine chironomid concentrations. Chironomid head capsules were hand-picked from freeze-dried as well as from wet sediments and reported concentrations are based on the total number of head capsules and the corresponding calculated dry weight. The datasets produced in this study are uploaded to the data repository Pangaea (https://doi.pangaea.de/10.1594/PANGAEA.908301).

If insufficient material was available to recover 50 head capsules (Heiri and Lotter, 2001; Quinlan and Smol, 2001), adjacent samples were merged before further analyses. However, even after merging it was not always possible to obtain a minimum count sum of 50 head capsules. In the section from 90 to 120 cm composite depth, samples were included in further analysis if the merged amount reached 40 head capsules. Below 130 cm composite depth, samples with a head capsule count of at least 25 were accepted. Because of the extremely low diversity, these samples were used despite the low count sum. Head capsules of the genus *Chironomus* that missed parts of the lateral teeth necessary for further identification were assigned to the two species groups *Chironomus anthracinus*-type and

Chironomus plumosus-type using the ratio of the identified head capsules prior to statistical analysis. Head capsules of the genus *Tanytarsus* that missed mandibles, but possessed an antennal pedastel without spur were listed as *Tanytarsus* “without spur”. Head capsules of *Tanytarsus* that also missed the antennal pedestal were listed as *Tanytarsus* indet., but included in the taxon *Tanytarsus* “without spur” for graphical representation. After excluding rare taxa (those with less than 2 samples with abundances higher than 2 %), square root transformed percentages of chironomid taxa were used to assign the samples to zones following a cluster analysis (Everitt, 2011). The number of statistically significant zones was determined with a broken-stick model (Bennett, 1996), and zonal boundaries are reported as ages rounded to the nearest century. Principal component analysis was used to summarise the data and to identify the most important taxa (ter Braak, 1983). Analyses were performed with R (R Core Team, 2016) using the package ‘vegan’ (Oksanen et al., 2016). Results were plotted using C2 (Juggins, 2014). We analysed the occurrence of regime shifts using the sequential algorithm presented by Rodionov (2004, 2006). This method allows the statistical detection of significant shifts time series based on a sequential t-test. We ran the algorithm using both the sample scores on PCA axis 1 and 2 as input, and explored a range of settings, in line with recommendations by Rodionov (2005). We here present the results for a test run with a significance level of 0.1, a cut-off length of 14 and a Huber's weight parameter of 1. Regime shifts were accepted as significant with a rate of change index of at least 0.95.

Results

A total of 118 samples were analysed, containing on average 34.6 chironomid head capsules (25.05 HC g^{-1} dry weight). Out of these, 22 samples were excluded from further analyses as they showed very low count sums. An additional 58 samples were merged into 13 samples to reach count sums suitable for further data exploration (Tab. S1). Fifty samples remained after this data processing procedure, of which seven samples contained less than 50 head capsules. No samples reached sufficient head capsule counts below 150 cm composite depth. We identified a total of 15 taxa in the record of Son Kol (Fig. 2). Five taxa were identified as being rare.

The chironomid record was devided into four zones, covering the intervals 150–124, 124–108, 108–92.5 and 92.5–12 cm, respecively (Fig. 2, Fig. S1). These correspond to the time windows of 6000-4900, 4900-4300, 4300-3700 and 3700-500 cal. yr BP, respectively. The lower two boundaries were statistically significant when compared to the a broken-stick model (Fig. S2). The third boundary was visually established based on minor changes in the chironomid record.

Zone I: 6000–4900 cal. yr BP (150–124 cm)

Psectrocladius sordidellus-type and *Cricotopus intersectus*-type dominate the assemblages of Zone I. The zone is characterized by the highest fluctuations along the core, both seen in between-sample fluctuations of dominant taxa, as well as in the head capsule concentration record, which ranges from samples void of chironomids to 304 HC/g dry sediment, the highest concentration of the record (Fig. 4). Charophyte oogonia and *Daphnia* ephippia occur (0.2-132.3 and 0.4-3.4 g dry $weight^{-1}$, respectively) in this zone. The sample scores on both PCA axis 1 and 2 are the lowest of the record and show a high variability.

Zone II: 4900–4300 cal. yr BP (124–108 cm)

In the second zone, the chironomid fauna is dominated by *Chironomus anthracinus*-type. *Psectrocladius sordidellus*-type and *Cricotopus intersectus*-type, the two taxa that were abundant during Zone I, disappeared almost completely at the onset of Zone II. Chironomid concentrations show only minor fluctuations, and generally low values during Zone II. No charophyte oogonia and only a single *Daphnia* ephippium were found in this zone. The scores of the samples on PCA axis 1 start a continuous increase in Zone II, while the scores on PCA axis 2 increase abruptly to reach the highest values of the record at the beginning of Zone II. With the exception of a slight dip around 4650 cal. yr BP, they remain high until an abrupt decrease occurs at the end of the zone.

Zone III: 4300–3700 cal. yr BP (108–92.5 cm)

After a second abrupt shift in the chironomid assemblages at ca. 4300 cal. yr BP *Tanytarsus* "without spur", *Tanytarsus gracilentus*-type and *Procladius* replaced *Chironomus anthracinus*-type. *Procladius* is the dominant taxon during the first part of Zone III, but shows declining abundances with time, whereas *Tanytarsus* "without spur" shows increasing abundances, becoming the dominant taxon. Chironomid concentrations, while showing only minor fluctuations, remain low at the zonal boundary, but start to increase at ca. 4000 cal. yr BP. While charophyte oogonia are still absent, *Daphnia* ephippia are present (0.1-0.7 g dry sediment^{-1}) throughout Zone III. The sample scores on PCA axis 1 continue to increase evenly, while the scores on PCA axis 2 are stable with values ranging between those of Zone I and Zone II.

Zone IV: 3700–500 cal. yr BP (92.5–12 cm)

The uppermost zone represents the longest and most stable zone of the record, showing dominance of *Tanytarsus gracilentus*-type and the more general morphotype *Tanytarsus* "without spur", accompanied by low percentages of *Procladius*. Chironomid concentrations continue to increase across the zonal boundary and remain stable above 30 HC g^{-1} dry sediment after ca. 3500 cal. yr BP. *Daphnia* ephippia were found only in the topmost sample. PCA scores remain at medium values throughout Zone IV.

Most of the variance of the chironomid data is explained by the first two PCA axes (in total 86.4 %), and three clusters of samples can be identified in a bi-plot showing PCA axis 1 and 2 (Fig. 3). *Tanytarsus gracilentus*-type and *Tanytarsus* "without spur" are most strongly associated with PCA axis 1 (eigenvalue of 26.3, 58.1 % variance explained), while *Psectrocladius sordidellus*-type, *Cricotopus intersectus*-type and *Chironomus anthracinus*-type are most strongly associated with PCA axis 2 (eigenvalue of 12.8, 28.3 % variance explained). Regime shift analysis revealed significant shifts at 4900, 4500–4300 and 3700 cal. yr BP, respectively. The exact timing of the shift at 4500–4300 cal. yr BP varied between the two PCA axes (4500 cal. yr BP in the analysis using the axis 1 scores, 4300 cal. yr BP in the analysis using axis 2 scores) and was only significant in PCA axis 1.

[Insert Fig. 2]

[Insert Fig. 3]

[Insert Fig. 4]

Discussion

Mid to late Holocene lake development

Son Kol developed from a closed, saline lake at 6000 cal. yr BP to the modern open, freshwater lake (Huang et al., 2014; Schwarz et al., 2017). Our chironomid record shows four zones during this time-interval (> 4900, 4900–4300, 4300–3700 and < 3700 cal. yr BP). These zones are similar to the four major zones previously recognized by Schwarz et al. (2017), who analysed diatoms, ostracods and stable isotope analysis in the same sediment sequence. The difference between the exact timings of the zonal boundaries established in this study and those by Schwarz et al. (2017) is only minor (up to 150 years), and is potentially due to differences in sampling density or proxy-response times.

Zone I (> 4900 cal. yr BP)

Psectrocladius sordidellus-type and *Cricotopus intersectus*-type were the most abundant taxa in the first zone. Both these Orthocladiinae morphotypes include species adapted to saline conditions (Plank, 2010; Zhang et al., 2007). Additionally, head capsule concentration showed high fluctuations during Zone I. If lake levels were lower than today, the coring site would have been closer to the shore and therefore more vulnerable to changing conditions such as river influence connected to differences in the sediment regime, thus potentially explaining the high variations observed in the chironomid concentrations. We therefore suggest that Son Kol was a shallow, saline lake during Zone I.

This chironomid-based palaeoenvironmental inference is in agreement with Schwarz et al. (2017) who infer a shallow, saline environment based on high conductivities reconstructed using a diatom-conductivity-transfer-function (8.2 mS cm^{-1}) as well as the dominance of the halophile ostracod species *Eucypris mareotica* (Fig. 4). The occurrences of single freshwater diatom valves opposing the otherwise dominating salinity indicators was interpreted as a result of freshwater inflow (Schwarz et al., 2017) which matches our interpretation of a shorter distance to the shore and thus higher influence of the tributaries.

Zone II (4900–4300 cal. yr BP)

Both cluster analysis and regime shift analysis show the occurrence of a statistically significant boundary at 4900 cal. yr BP. This result is consistent between regime shift analyses using both PCA axis 1 and axis 2 scores, and tests run using different statistical settings. The onset of Zone II at 4900 cal. yr BP is characterised by an abrupt increase in *Chironomus anthracinus*-type, a chironomid morphotype which can occur under a range of environmental conditions. Due to the large range of habitat conditions suitable for *C. anthracinus*-type, it is hard to provide an ecological interpretation of the environmental conditions during Zone II based on the chironomid data alone. A chironomid-based interpretation of palaeoenvironmental conditions during Zone II is further hampered by the fact that the generalist genus *Procladius* (Vallenduuk and Moller Pillot, 2013) is the only other chironomid taxon that occurred in abundances over 10 % during Zone II. The comparison of the chironomid fauna of Zone II to the other zones shows striking differences in the habitat preferences of the dominant taxa. In contrast to the sediment-bound *C. anthracinus*-type that was dominant during Zone II (Moller Pillot, 2013a), the morphotypes (*Cricotopus intersectus*-type, *Psectrocladius sordidellus*-type and *Tanytarsus gracilentus*-

type) that were abundant during Zones I and III are all associated with macrophyte vegetation (Brodersen et al., 2001; Ives et al., 2008; Lindegaard et al., 1979; Moller Pillot, 2013b). We suggest that the disappearance of these macrophyte-associated taxa in favour of the sediment-bound *C. anthracinus*-type that (Moller Pillot, 2013a) at the onset of Zone II could have been caused by a decline of the aquatic macrophyte vegetation. Alternatively, the strong could be explained by other factors such as low oxygen conditions (Moller Pillot, 2013a), eutrophication (Meriläinen et al., 2000), or heavy metal pollution (Mocq et al., 2018). However, such conditions are unlikely to have occurred in the relatively shallow and oligotrophic Son Kol, which even at present is not under high anthropogenic pressure. Furthermore, a high pH resulting from e.g. increased fluvial input of carbonate rocks from the catchment could also have potentially led to high abundances of *C. anthracinus*-type (Moller Pillot, 2013a). However, as *Tanytarsus gracilentus*-type, the chironomid taxon dominating the following zones, is also adapted to high pH values, a shift to higher pH values is unlikely to be the only driver of the abrupt ecosystem shifts observed at the start and end of Zone II.

The ostracod assemblages were dominated by *Limnocythere inopinata*, a pH-independent generalist as well (Caballero et al., 2003; Külköylüoğlu, 2005), and a lack of sufficient preserved diatom remains only confirmed conditions harsh for aquatic life, but did not provide further insight into the environmental conditions at that time (Schwarz et al., 2017; Fig. 4). However, some information can be gained from the geochemical analyses by Lauterbach et al. (2014), in particular from the total organic carbon (TOC) content, indicating the lowest productivity of the entire record during this interval, and the $\delta^{15}N$ values, which showed the highest values during this zone (Fig. 4). While there are several reasons for high $\delta^{15}N$ values in general, eg denitrification processes in an anoxic hypolimnion, increased aquatic production or high evaporation, increased input of terrestrial organic material, brought by fluvial input due to increased precipitation, hence increased Westerly strength, was proposed as the only plausible cause for Son Kol in this case (Lauterbach et al., 2014). The sediment input, combined with high wind velocities during this phase of increased Westerly strength, might have resulted in high turbidity, which in turn could explain the inferred low lake-internal productivity. High turbidity could also explain the low diatom concentrations during Zone II found by Schwarz et al. (2017), because the low availability of sunlight could have led to low diatom production and the dispersed sediment particles might, in particular under high pH, have damaged the diatom valves. Increased turbidity could have caused a decline of macrophyte vegetation and could therefore explain the dominance of *C. anthracinus*-type in Zone II (Blindow et al., 2002; Ibelings et al., 2007) and would further explain the low TOC values in Zone II.

We therefore argue that increased turbidity between 4900 and 4300 cal. yr BP could have hampered macrophyte growth, which might have further increased turbidity (eg through wave-driven mobilization of now more unconsolidated lake bottom sediments) until this self-enforcing process led to a collapse of macrophyte vegetation. Scheffer (1993) showed, even though driven by eutrophication instead of sediment input and strong wind velocities, how the interplay of turbidity and macrophyte growth can lead to abrupt shifts between turbid and clear stable states. Indicators for the clear state were in particular Charophyta and Cladocera (Scheffer et al., 1993, 2003; van den Berg et al., 1998), whose remains were concordantly found in Zone I, but were absent in Zone II (Fig. 4). The observed delay in the shift of bioindicators compared to that in $\delta^{15}N$ supports the hypothesis of alternative stable

states, because the ecosystem pressure applied by fluvial input and high wind speeds needed to add up to trigger the cascade which than abruptly changed the ecosystem state. The opposing effect of decreasing Westerly strength triggering the cascade of decreasing turbidity followed by macrophyte recolonization leading to even lower turbidity (Ibelings et al., 2007; Scheffer et al., 2003; van Nes et al., 2016) might have driven the second abrupt change.

Especially noticeable is the comparison of TOC and $\delta^{15}N$ to the scores of the chironomid based PCA axis 2. The pattern of all three graphs, even though reversed for TOC, throughout Zone II is very similar, showing an abrupt increase, a dip in the middle of the zone, and an abrupt decrease, the timing of increase and decrease however, is delayed in the PCA axis 2 (Fig. 4). We interpret the difference between the timing of allochthonous input indicated by the δ15N values, and the changes seen in the bioindicators to reflect a delayed response of the lake ecosystem to the change in strength of the Westerlies.

Zone III (4300–3700 cal. yr BP)

The zonal boundary at 4300 cal. yr BP is statistically significant when compared to a broken stick model, and regime shift analysis furthermore suggests the occurrence of an abrupt shift between 4500 and 4300 cap yr BP, although the exact timing of the shift varies between different model runs. The onset of Zone III is characterised by a decrease in *C. anthracinus*-type in favour of *Procladius* and *Tanytarsus gracilentus*-type. Both these chironomid taxa indicate mesohaline conditions (Plank 2010), and the abundant presence of the free swimming genus *Procladius* (Vallenduuk and Moller Pillot, 2013) and the macrophyte-associated *T. gracilentus*-type (Ives et al., 2008; Lindegaard et al., 1979) during Zone III could reflect a re-established clear water state with abundant macrophyte vegetation. Zone III is furthermore characterized by low chironomid head capsule concentrations, which increased throughout the zone. The increase in head capsule concentrations is accompanied by an increase in the relative abundance of *Tanytarsus gracilentus*-type. We therefore interpret this increase in concentrations as a result of increasing productivity of *T. gracilentus*-type rather than as a decrease of productivity of *Procladius*. This development might have been connected to a stabilization of the conditions connected to the opening of the lake system.

The chironomid-based inference of a shift toward less saline conditions is in line with the diatom-based conductivity reconstruction (1.5 mS cm^{-1}) and the dominance of the ostracod species *Candona neglecta* (Schwarz et al., 2017, Fig. 4). The reduced salinity can be interpreted as a result of a lake level rise during the phase of increased Westerly strength.

Zone IV (< 3700 cal. yr BP)

The zonal boundary between chironomid Zones III and IV is not statistically significant, but was visually established to highlight the minor changes observed in the chironomid diagram around 3700 cal. yr BP. From this time onward, *Tanytarsus gracilentus*-type strongly dominated the chironomid assemblages (average abundances 92.4 %). Abundances of *T. gracilentus*-type that exceed 90 % are currently only observed in the fresh alkaline (pH of 8.1-10) Icelandic lake Mývatn (Ives et al., 2008; Opfergelt et al., 2004). The chironomid results therefore suggest alkaline, freshwater to mesohaline conditions from ca. 3700 cal. yr. BP onward.

The chironomid-based interpretation is in line with the results by Schwarz et al. (2017) who

reconstructed freshwater conditions in a deeper, open lake. The proportion of planktonic diatoms in this zone was very high and its increase around the zone boundary (Fig. 4) was the main signal that allowed the interpretation that the lake level rose and the lake system opened. Whereas our chironomid record shows little variability from 3700 cal. yr BP onward, Schwarz et al. (2017) identified four separate zones based on changes in the diatom and ostracod communities of the lake. We hypothesise that the strong dominance of *T. gracilentus* obscured the registration of environmental changes that affected the diatom and ostracod assemblages.

Tipping points

Many definitions exist concerning the term “tipping point”. We use the definition of an abrupt change triggered by minor changes tipping the system over a threshold where self-enforcing processes lead the system to another stable state (Lenton et al., 2008; van Nes et al., 2016). In our study we found two abrupt changes, both showing shifts to alternative stable system states that lasted for more than 500 years.

The main environmental trigger resulting in the first abrupt change at 4900 cal. yr BP was the increased influence of the Westerlies causing increased water and sediment input into the lake as well as high wind velocities. These factors led to increased turbidity followed by macrophyte decline. While such an increased influence of the Westerlies at Son Kol has been found several times during the last 6000 years (Lauterbach et al., 2014; Schwarz et al., 2017), it only once led to an ecosystem-wide abrupt change. A probable explanation is that only in this case the environmental pressure of turbidity was high enough to trigger a decline of macrophyte vegetation extensive enough to tip the system into the self-enforcing cascade of further increasing turbidity leading to the complete collapse of macrophyte vegetation. Alternate lake states coupled to macrophyte vegetation and turbidity have been observed in the context of eutrophication and subsequent ecosystem recovery in Lake Veluwe, Netherlands (Ibelings et al., 2007; Scheffer 1993, 2003), and a similar process under westerly wind induced turbidity is plausible (Fig. 5).

The opposite mechanism took place at 4300 cal. yr BP, when the Westerlies influence declined forming an environmental trigger that ultimately led to an abrupt ecosystem change. The lower amounts of precipitation associated with the decreasing influence of Westerlies led to less water and sediment input into the lake and, combined with lower wind velocities, resulted in lower turbidity in the water column. At one point the resulting environmental pressure on the submerged plant vegetation was low enough to allow the recolonization of the lake, tipping the system over the threshold into the self-enforcing cascade of increasing vegetation cover leading to lower turbidity until a clear water state was reached once more.

In both cases, we see environmental triggers, namely changes in the intensity of Westerlies, leading to environmental pressure starting self-enforced within-lake cascades driven by turbidity and macrofauna disappearance or expansion. These sequences are in line with the criteria of tipping points as suggested by Lenton et al. (2008) and van Nes et al. (2016). Our interpretation is further supported by the delayed timing of the ecosystem change compared to the shift in $\delta^{15}N$-values, because these values display the environmental pressure applied to the system and the delayed response of the ecosystem demonstrates how the pressure had to rise until it crossed the tipping point starting the abrupt ecosystem reaction.

[Insert Fig. 5]

Comparison against other records

Environmental changes between about 4900 and 4500 cal. yr. BP have been reconstructed for many different Central Asian archives. The underlying conditions characterizing these changes though, are different. While most results indicate cooling, the precipitation signal reveals a more heterogeneous spatio-temporal pattern, strongly depending on the locality. In many Tibetan lakes, the cooling in this interval was associated with dry conditions (Doberschütz et al., 2014; Ma et al., 2019; Morinaga et al., 1993; Shi et al., 2017; Xu et al., 2019a). A similar picture was found in several studies from the Southern Altai (Li et al., 2011; Wang and Zhang, 2019; Xu et al., 2019b), as well as Southern Mongolia (Felauer et al., 2012). In contrast, a shift to wetter conditions was found in studies of the Southern (Zhang et al., 2016, 2018), Western and Northern Altai mountains (Ilyashuk and, Ilyashuk, 2007; Zhang and Feng, 2018) and the Tian Shan (Beer et al., 2007; Huang et al., 2015).

The regional differences in precipitation changes during this interval were attributed to the influence of the dominating wind system: under Monsoon influence, the trend is connected to dry conditions, whilst under Westerlies influence it is related to humid conditions (Rao et al., 2019). Our Son Kol reconstruction, which shows a wet phase from 4900 to 4300 cal. y. BP and continuing humid conditions thereafter, fits the model of a dominant influence of the Westerlies (Huang et al., 2014; Mathis et al., 2014; Schwarz et al., 2017).

While the time window 4900-4300 cal. yr BP covers both abrupt changes identified in our study, there are not many records from Central Asia that also show an environmental change around 3700 cal. yr BP, where a third, more gradual, transition is observed in the Son Kol record. Han et al. (2019) found evidence for major sand storms in the Tarim Basin ca. 3500 cal. yr BP, connecting it to a southward shift of the Westerlies. While a connection to changes in the Westerlies regime might have partly influence the lake system at this time, we consider local effects, possibly the opening of the lake system, as the more likely cause of the Son Kol ecosystem transition at ca. 3700 cal. yr BP.

Conclusions

We produced a high-resolution palaeoecological and palaeoenvironmental record for Lake Son Kol. The main aim of this study was to assess the occurrence and ecosystem cascades characterizing tipping points as well as their distinction from other environmental changes, and our results show prominent ecosystem shifts at two tipping points (4900 and 4300 cal. yr BP) and one gradual shift (3700 cal. yr BP) in the development of the central Kyrgyzstan lake Son Kol from a saline to a freshwater lake. These results are in line with previous studies on diatoms and ostracods (Schwarz et al., 2017), as well as geochemical analyses (Lauterbach et al., 2014). We postulate that a phase of increased Westerly strength causing increased water and sediment input, in combination with high wind velocities to be the trigger of both ecosystem-wide tipping points. As driver we postulate the self-enforcing cascade of increasing turbidity and declining submerged macrophyte cover at the first and the opposite process at the second tipping point (Fig. 5).

These conditions are represented by abrupt changes from the macrophyte-associated salinity indicators *Cricotopus intersectus*-type and *Psectrocladius sordidellus*-type over the sediment-bound *Chironomus anthracinus*-type to the again macrophyte associated alkaline but fresh-mesohaline conditions indicating *Tanytarsus gracilentus*-type. While salinity plays

an important role distinguishing the chironomid, ostracod and diatom taxa before 4900 and after 4300 cal. yr BP, it cannot explain the assemblages in-between. The gradual change (3700 cal. yr BP) reflects the transition from a closed to an open lake system and is represented by increasing chironomid head capsule concentrations and *Tanytarsus gracilentus*-type abundances and fits the increase of planktonic diatoms recognized by Schwarz et al. (2017).

Our study demonstrates in detail how ecosystems can shift in reaction to an external trigger and how self-enforcing cascades can generate ecosystem-wide tipping points.

Acknowledgements

We thank Martina Stebich for data contribution and discussion. We thank two anonymous reviewers and editor professor Vivienne Jones for their constructive and critical reviews of the manuscript that helped to improve the manuscript.

Declaration of conflicting interests

The authors declare that there is no conflict of interest.

Funding

The authors disclosed receipt of the following financial support for the research of this article: This work was supported by the German Federal Ministry of Education and Research (BMBF) through funding the projects “CADY – Central Asian Climate Dynamics” (03G0813) and “CAHOL – Holozäne Klimaschwankungen in Zentralasien“ (03G0864).

Literature

Academy of Science of the Kyrgyz SSR (1987) *Atlas of the Kyrgyz Soviet Socialistic Republic. Volume 1: Natural Conditions and Resources*. Moscow: State Agency for Cartography and Geodesy, Central Directorate for Geodesy and Cartography, Council of Ministers of the USSR.

Aizen EM, Aizen VB, Melack JM et al. (2001) Precipitation and atmospheric circulation patterns at mid-latitudes of Asia. *International Journal of Climatology* 21(5): 535–556.

Aizen VB, Aizen EM, Melack JM. et al. (1997) Climatic and Hydrologic Changes in the Tien Shan, Central Asia. *Journal of Climate* 10(6): 1393–1404.

Alivernini M, Lai Z, Frenzel P et al. (2018) Late Quaternary lake level changes of Taro Co and neighbouring lakes, southwestern Tibetan Plateau, based on OSL dating and ostracod analysis. *Global and Planetary Change* 166: 1–18.

Andersen T, Carstensen J, Hernández-García E. et al. (2009) Ecological thresholds and regime shifts: approaches to identification. *Trends in ecology & evolution* 24(1): 49–57.

Battarbee RW (2000): Palaeolimnological approaches to climate change, with special regard to the biological record. *Quaternary Science Reviews* 19: 107–124.

Beer R, Heiri O and Tinner W (2007) Vegetation history, fire history and lake development recorded for 6300 years by pollen, charcoal, loss on ignition and chironomids at a small lake in southern Kyrgyzstan (Alay Range, Central Asia). *The Holocene* 17(7): 977–985.

Bennett KD (1996) Determination of the number of zones in a biostratigraphical sequence. *New Phytologist* 132(1): 155–170.

Bitušík P and Hamerlík L. (2014) *Prirucka na urcovanie lariev pakomarov (Diptera: Chironomidae) Slovenska. Cast 2. Tanypodinae. (Identification key for Tanypodinae)*. Banska Bystrica: Belianum.

Blindow I, Hargeby A and Andersson G (2002) Seasonal changes of mechanisms maintaining clear water in a shallow lake with abundant Chara vegetation. *Aquatic Botany* 72(3–4): 315–334.

Brodersen KP, Odgaard BV, Vestergaard O et al. (2001) Chironomid stratigraphy in the shallow and eutrophic Lake Sobygaard, Denmark: Chironomid-macrophyte co-occurrence. *Freshwater Biology* 46(2): 253–267.

Bronk Ramsey C (2008) Deposition models for chronological records. *Quaternary Science Reviews* 27(1–2): 42–60.

Bronk Ramsey C (2009) Bayesian Analysis of Radiocarbon Dates. *Radiocarbon* 51(1): 337–360.

Brooks SJ (2006): Fossil midges (Diptera Chironomidae) as palaeoclimatic indicators for the Eurasian region. *Quaternary Science Reviews* 25: 1894–1910.

Brooks SJ and Birks HJB (2000): Chironomid-inferred late-glacial and early-Holocene mean July air temperatures for Kråkenes Lake, western Norway. *Journal of Paleolimnology* 23(1): 77–89.

Brooks SJ, Langdon PG and Heiri O (2007) *The identification and use of palaearctic chironomidae larvae in palaeoecology. QRA Technical Guide 10*. London: Quaternary Research Association.

Caballero M, Vilaclara G, Rodríguez A et al. (2003) Short-term climatic change in lake sediments from lake Alchichica, Oriental, Mexico. *Geofísica Internacional* 42(3): 529–537.

Charles DF, Whitehead DR, Engstrom, DR et al. (1987) Paleolimnological evidence for recent acidification of Big Moose Lake, Adirondack Mountains, N.Y. (USA). *Biogeochemistry* 3: 167–296.

Chen J, Chen F, Zhang E et al. (2009) A 1000-year chironomid-based salinity reconstruction from varved sediments of Sugan Lake, Qaidam Basin, arid Northwest China, and its palaeoclimatic significance. *Chinese Science Bulletin* 54(20): 3749–3759.

Cheng H, Zhang PZ, Spötl C et al. (2012) The climatic cyclicity in semiarid-arid central Asia over the past 500,000 years. *Geophysical Research Letters* 39(1).

de Grave J, Glorie S, Buslov MM et al. (2011) The thermo-tectonic history of the Song-Kul plateau, Kyrgyz Tien Shan: Constraints by apatite and titanite thermochronometry and zircon U/Pb dating. *Gondwana Research* 20(4): 745–763.

Doberschütz S, Frenzel P, Haberzettl T et al. (2014) Monsoonal forcing of Holocene paleoenvironmental change on the central Tibetan Plateau inferred using a sediment record from Lake Nam Co (Xizang, China). *Journal of Paleolimnology* 51(2) 253–266.

Engels S, Cwynar LC, Rees, ABH et al. (2012) Chironomid-based water depth reconstructions: an independent evaluation of site-specific and local inference models. *Journal of Paleolimnology* 48(4): 693–709.

Everitt B (2011) *Cluster analysis, 5. edition*. Chichester: Wiley.

Felauer T, Schlütz F, Murad W et al. (2012) Late Quaternary climate and landscape evolution in arid Central Asia: A multiproxy study of lake archive Bayan Tohomin Nuur¢, Gobi desert, southern Mongolia. *Journal of Asian Earth Sciences* 48: 125–135.

Flower RJ (1993) Diatom preservation: Experiments and observations on dissolution and breakage in modern and fossil material. *Hydrobiologia* 269(1): 473–484.

Greffard MH, Saulnier-Talbot E and Gregory-Eaves I (2012) Sub-fossil chironomids are significant indicators of turbidity in shallow lakes of northeastern USA. *Journal of Paleolimnology* 47(4): 561–581.

Grodzins M (1958) *The metropolitan area as a racial problem*. Pittsburgh: University of Pittsburgh Press.

Han W, Lü S, Appel E et al. (2019) Dust storm outbreak in central Asia after ~3.5 kyr BP. *Geophysical Research Letters* 46(13): 7624–7633.

Heiri O and Lotter AF (2001) Effect of low count sums on quantitative environmental reconstructions: an example using subfossil chironomids. *Journal of Paleolimnology* 26(3): 343–350.

Huang X, Chen C, Jia W et al. (2015): Vegetation and climate history reconstructed from an alpine lake in central Tienshan Mountains since 8.5 ka BP. *Palaeogeography, Palaeoclimatology, Palaeoecology* 432: 36–48.

Huang X, Oberhänsli H, von Suchodoletz, H et al. (2014) Hydrological changes in western Central Asia (Kyrgyzstan) during the Holocene as inferred from a palaeolimnological study in lake Son Kul. *Quaternary Science Reviews* 103: 134–152.

Ibelings BW, Portielje R, Lammens, EHRR et al. (2007) Resilience of Alternative Stable States during the Recovery of Shallow Lakes from Eutrophication: Lake Veluwe as a Case Study. *Ecosystems* 10(1): 4–16.

Ilyashuk B and Ilyashuk E (2007) Chironomid record of Late Quaternary climatic and environmental changes from two sites in Central Asia (Tuva Republic, Russia) – local, regional or global causes? *Quaternary Science Reviews* 26(5–6): 705–731.

Ives AR, Einarsson A, Jansen VAA et al. (2008) High-amplitude fluctuations and alternative dynamical states of midges in Lake Myvatn. *Nature* 452(7183): 84–87.

Jarvis A, Reuter HI, Nelson A et al. (2008) Hole-filled SRTM for the globe Version 4. Available from the CGIAR-CSI SRTM 90m Database (http://srtm.csi.cgiar.org).

Juggins S (2014) C2 data analysis. Version 1.7.7. Available at: https://www.staff.ncl.ac.uk/stephen.juggins/software/C2Home.htm (accessed 05 November 2019)

593 Külköylüoğlu O (2005) Ecology and Phenology of Freshwater Ostracods in Lake Gölköy
594 (Bolu, Turkey). *Aquatic Ecology* 39(3): 295–304.

595 Lauterbach S, Witt R, Plessen B et al. (2014) Climatic imprint of the mid-latitude Westerlies
596 in the Central Tian Shan of Kyrgyzstan and teleconnections to North Atlantic climate
597 variability during the last 6000 years. *The Holocene* 24(8): 970–984.

598 Lees K, Pitois S, Scott C et al. (2006) Characterizing regime shifts in the marine
599 environment. *Fish Fisheries* 7(2): 104–127.

600 Lenton TM, Held H, Kriegler E et al. (2008) Tipping elements in the Earth's climate system.
601 *Proceedings of the National Academy of Sciences of the United States of America*
602 105(6): 1786–1793.

603 Li X, Zhao K, Dodson J et al. (2011) Moisture dynamics in central Asia for the last 15 kyr:
604 New evidence from Yili Valley, Xinjiang, NW China. *Quaternary Science Reviews*
605 30(23–24): 3457–3466.

606 Lindegaard C and Jónasson PM (1979) Abundance, Population Dynamics and Production of
607 Zoobenthos in Lake Mývatn, Iceland. *Oikos* 32(1–2): 202–207.

608 Ma Q, Zhu L, Lü X et al. (2019) Late glacial and Holocene vegetation and climate variations
609 at Lake Tangra Yumco, central Tibetan Plateau. *Global and Planetary Change* 174:
610 16–25.

611 Mathis M, Sorrel P, Klotz S et al. (2014) Regional vegetation patterns at lake Son Kul reveal
612 Holocene climatic variability in central Tien Shan (Kyrgyzstan, Central Asia).
613 *Quaternary Science Reviews* 89:169–185.

614 Meriläinen JJ, Hynynen J, Palomäki A et al. (2000) Importance of diffuse nutrient loading
615 and lake level changes to the eutrophication of an originally oligotrophic boreal lake: a
616 palaeolimnological diatom and chironomid analysis. *Journal of Paleolimnology* 24(3):
617 251–270.

618 Mischke S and Wünnemann B (2006): The Holocene salinity history of Bosten Lake
619 (Xinjiang, China) inferred from ostracod species assemblages and shell chemistryr
620 Possible palaeoclimatic implications. *Quaternary International* 154–155: 100–112.

621 Mocq J and Hare L (2018) Influence of Acid Mine Drainage, and Its Remediation, on
622 Lakewater Quality and Benthic Invertebrate Communities. *Water, Air & Soil Pollution*
623 229(28): 1–15.

624 Moller Pillot HKM (2013a) *Biology and ecology of the Chironomini, 2. edition.* Zeist: KNNV
625 Publishing.

626 Moller Pillot HKM (2013b) *Chironomidae Larvae, Vol. 3: Orthocladiinae*. Zeist: KNNV
627 Publishing.

628 Morinaga H, Itota C, Isezaki N et al. (1993) Oxygen-18 and carbon-13 records for the last
629 14,000 years from Lacustrine carbonates of Siling-Co (Lake) in the Qinghai-Tibetan
630 Plateau. *Geophysical Research Letters* 20(24): 2909–2912.

631 Motta L, and Massaferro J (2019) Climate and site-specific factors shape chironomid
632 taxonomic and functional diversity patterns in northern Patagonia. *Hydrobiologia*
633 839(1): 131–143.

634 Oksanen, JFG, Blanchet R, Kindt P et al. (2016) Vegan: Community Ecology Package. R
635 Package Vers. 2.4e1. Accessible at: https://CRAN.R-project.org/package=vegan
636 (accessed at 05 November 2019)

637 Opfergelt S, Eiriksdottir ES, Burton KW et al. (2004) Quantifying the impact of freshwater
638 diatom productivity on silicon isotopes and silicon fluxes: Lake Myvatn, Iceland. *Earth*
639 *and Planetary Science Letters* 305(1–2): 73–82.

640 Pacton M, Sorrell P, Bevillard B et al. (2015) Sedimentary facies analyses from nano- to
641 millimetre scale exploring past microbial activity in a high-altitude lake (Lake Son Kul,

642 Central Asia). *Geological Magazine* 152(5): 902–922.

643 Plank A (2010) *Chironomid-based inference models for Tibetan lakes aided by a newly*
644 *developed chironomid identification key*. PhD Thesis, Freie Universität Berlin, GER

645 Quinlan R and Smol JP (2001) Setting minimum head capsule abundance and taxa deletion
646 criteria in chironomid-based inference models. *Journal of Paleolimnology* 26(3): 327–
647 342.

648 R Core Team (2016): *R: a Language and Environment for Statistical Computing*. Vienna: R
649 Foundation for Statistical Computing.

650 Randsalu-Wendrup L, Conley DJ, Carstensen J et al. (2014) Combining limnology and
651 palaeolimnology to investigate recent regime shifts in a shallow, eutrophic lake.
652 *Journal of Paleolimnology* 51: 437–448.

653 Randsalu-Wendrup L, Conley DJ, Carstensen J et al. (2016) Paleolimnological records of
654 regime shifts in lakes in response to climate change and anthropogenic activities.
655 *Journal of Paleolimnology* 56: 1–14.

656 Rao Z, Wu D, Shi F et al. (2019) Reconciling the 'westerlies' and 'monsoon' models: A new
657 hypothesis for the Holocene moisture evolution of the Xinjiang region, NW China.
658 *Earth-Science Reviews* 191: 263–272.

659 Reimer PJ, Baillie MGL, Bard E et al. (2009) IntCal09 and Marine09 radiocarbon age
660 calibration curves, 0–50,000 years cal BP. *Radiocarbon* 51: 1111–1150.

661 Rieradevall M, Brooks SJ (2001) An identification guide to subfossil Tanypodinae larvae
662 (Insecta: Diptera: Chrironomidae) based on cephalic setation. *Journal of*
663 *Paleolimnology* 25(1): 81–99.

664 Rippey B, Mc Sorley C (2009) Oxygen depletion in lake hypolimnia. *Limnology and*
665 *Oceanography* 54(3): 905–916.

666 Rodionov SN (2004) A sequential algorithm for testing climate regime shifts. *Geophysical*
667 *Research Letters* 31(9): L09204.

668 Rodionov SN (2005) Detecting regime shifts in the mean and variance: Methods and specific
669 examples. In Velikova V, Chipev N editors, *Large-Scale Disturbances (Regime Shifts)*
670 *and Recovery in Aquatic Ecosystems: Challenges for Management Toward*
671 *Sustainability*, UNESCO-ROSTE/BAS Workshop on Regime Shifts, 14-16 June 2005,
672 Varna, Bulgaria, 68-72.

673 Rodionov SN (2006) The use of prewhitening in climate regime shift detection, Geophysical
674 Research Letters 33(12): L12707.

675 Scheffer M, Hosper SH, Meijer, ML et al. (1993) Alternative equilibria in shallow lakes.
676 *Trends in ecology & evolution* 8(8): 275–279.

677 Scheffer M, Portielje R and Zambrano L (2003) Fish facilitate wave resuspension of
678 sediment. *Limnology and Oceanography* 48(5): 1920–1926.

679 Schwalb A, Hadorn P, Thew N et al. (1998) Evidence for Late-Glacial and Holocene
680 environmental changes from subfossil assemblages and sediments of Lake
681 Neuchâtel, Switzerland. *Palaeogeography, Palaeoclimatology, Palaeoecology* 140:
682 307-323.

683 Schwarz A, Turner F, Lauterbach S et al. (2017) Mid- to late Holocene climate-driven regime
684 shifts inferred from diatom, ostracod and stable isotope records from Lake Son Kol
685 (Central Tian Shan, Kyrgyzstan). *Quaternary Science Reviews* 177: 340–356.

686 Shi X, Kirby E, Furlong KP et al. (2017) Rapid and punctuated Late Holocene recession of
687 Siling Co, central Tibet. *Quaternary Science Reviews* 172: 15–31.

688 Shnitnikov AV (1980) *Ozera Tian-shanya I Ikh Istoriya (Lakes of the Tian Shan and Their*
689 *History)*. Leningrad: Nauka.

690 ter Braak CJF (1983) Principal Components Biplots and Alpha and Beta Diversity. *Ecology*
691 64(3): 454-462.

692 Vallenduuk HJ and Moller Pillot HKM (2013) *General ecology and Tanypodinae, 2. edition.*
693 Zeist: KNNV Publishing Zeist.

694 van den Berg M, Scheffer M, Coops H et al. (1998) The role of Characean algae in the
695 management of eutrophic lakes. *Journal of Phycology* 34(5): 750–756.

696 van Nes EH, Arani BMS, Staal A et al. (2016) What Do You Mean, 'Tipping Point'? *Trends in*
697 *ecology & evolution* 31(12): 902–904.

698 Wang W and Zhang D (2019) Holocene vegetation evolution and climatic dynamics inferred
699 from an ombrotrophic peat sequence in the southern Altai Mountains within China.
700 *Global and Planetary Change* 179: 10–22.

701 Winkler MG and Wang PK (1993): The Late-Quaternary vegetation and climate of China. In:
702 Wright HE, Kutzbach JE, Webb T et al. (eds.) *Global Climates since the Last Glacial*
703 *Maximum*. Minneapolis: University of Minnesota Press pp. 221–264.

704 Xu H, Zhou K, Lan J et al. (2019b) Arid Central Asia saw mid-Holocene drought. *Geology*
705 47(3): 255–258.

706 Xu T, Zhu L, Lü X et al. (2019a) Mid- to late-Holocene paleoenvironmental changes and
707 glacier fluctuations reconstructed from the sediments of proglacial lake Buruo Co,
708 northern Tibetan Plateau. *Palaeogeography, Palaeoclimatology, Palaeoecology* 517:
709 74–85.

710 Zhang D and Feng Z (2018) Holocene climate variations in the Altai Mountains and the
711 surrounding areas: A synthesis of pollen records. *Earth-Science Reviews* 185: 847–
712 869.

713 Zhang E, Chang J, Cao Y et al. (2017) A chironomid-based mean July temperature
714 inference model from the south-east margin of the Tibetan Plateau, China. *Climate of*
715 *the Past* 13(3): 185–199.

716 Zhang E, Jones R, Bedford A et al. (2007) A chironomid-based salinity inference model from
717 lakes on the Tibetan Plateau. *Journal of Paleolimnology* 38(4): 477–491.

718 Zhang Y, Meyers PA, Liu X et al. (2016) Holocene climate changes in the central Asia
719 mountain region inferred from a peat sequence from the Altai Mountains, Xinjiang,
720 northwestern China. *Quaternary Science Reviews* 152: 19–30.

721 Zhang Y, Yang P, Tong C et al. (2018) Palynological record of Holocene vegetation and
722 climate changes in a high-resolution peat profile from the Xinjiang Altai Mountains,
723 northwestern China. *Quaternary Science Reviews* 201: 111–123.

724 Zhao Y, Sayer CD, Birks HH et al. (2006) Spatial Representation of Aquatic Vegetation by
725 Macrofossils and Pollen in a Small and Shallow Lake. *Journal of Paleolimnology* 35(2):
726 335–350.

727

728

Supplementary

Tab. S1: Excluded and merged samples due to low head capsule concentration

Excluded samples:

123, 123.5, 124, 140, 140.5, 141,141.5, 142, 142.5, 143, 143.5, 144, 144.5, 145, 145.5, 146, 152.5, 157.5, 163, 165, 167.5, 170 cm

Merged samples:

91-95 cm	(5 samples, total count sum 53.5 head capsules)
96-100 cm	(6 samples, total count sum 40 head capsules)
100.5-105 cm	(10 samples, total count sum 41 head capsules)
105.5-107.5 cm	(5 samples, total count sum 42 head capsules)
108-110.5 cm	(5 samples, total count sum 67 head capsules)
111.5-112 cm	(2 samples, total count sum 52.5 head capsules)
112.5-113.5 cm	(3 samples, total count sum 64 head capsules)
114-115.5 cm	(4 samples, total count sum 57 head capsules)
116-118 cm	(5 samples, total count sum 56 head capsules)
121.5-122.5 cm	(3 samples, total count sum 53 head capsules)
130.5-132 cm	(4 samples, total count sum 32.5 head capsules)
146.5-147 cm	(2 samples, total count sum 26 head capsules)
148.5-150 cm	(4 samples, total count sum 29 head capsules)

[Insert Fig. S1]

[Insert Fig. S2]

Figure captions

Fig. 1: Left: Bathymetric map of Lake Son Kol (isobaths with corresponding water depths in meters below lake level; modified after Academy of Science of the Kyrgyz SSR, 1987) and relief of the surrounding area (elevations in meters above sea level). The coring site is indicated by a white circle (modified after Schwarz et al., 2017). Right: Topographic maps of Central Asia (top panel) and Kyrgyzstan with neighboring countries (CHN – China, KZ – Kazakhstan, UZ – Uzbekistan, TJ – Tajikistan) and the location of Son Kol (bottom panel). The relief map of Kyrgyzstan is based on the CGIAR-CSI SRTM 90 m (3 arcsec) digital elevation data (Version 4) of the NASA Shuttle Radar Topography Mission (Jarvis et al., 2008).

Fig. 2: Summary diagram showing chironomid taxa (in % of the head capsule sum), sample count sums (samples < 50 head capsules) and chironomid head capsule concentration against depth (cm), with a secondary age-scale (cal. yr BP) plotted for comparison. The width of the chironomid sample bars corresponds to the thickness of the (merged) samples. Zonation based on chironomid assemblages. Samples below 150 cm are excluded due to their low count sums.

Fig. 3: Principal components analysis(PCA) biplot of abundant chironomid taxa (arrows) and samples (circles). The variance explained by the first and second axis is 58.1 and 29.3 %, respectively. Blue circles mark the chironomid assemblage zones.

Fig. 4: Summary diagram of the paleoenvironmental development of Son Kol. From left to right: picture of the sediment record, δ15N- and TOC-values (Lauterbach et al., 2014), selected ostracod taxa, the planktonic-benthic diatom ratio and the diatom-inferred conductivity record (Schwarz et al., 2017); PCA axes 1 and 2 scores, presence of Charophyte oogonia and Daphnia ephippia (this study). Horizontal lines in the PCA-records indicate statistically significant regime shifts (see text for further information). Data plotted against depth (cm) with a secondary age-scale (cal. yr BP) shown for comparison. Zonation based on chironomid assemblages. Samples below 150 cm are excluded due to their low count sums.

Fig. 5: Schematic representation of the Son Kol ecosystem response to a) an increase in the strength of the Westerlies at 4900 cal. yr BP and b) a decrease in strength of the Westerlies at 4300 cal. yr BP. We propose that this change in the strength of the Westerlies can be seen as an external trigger that subsequently led to changes in turbidity, which themselves acted as a driver affecting the macrophyte population of the lake, and, ultimately, the ecosystem state.

Fig. S1: Cluster analysis based on square-root transformed percentages of non-rare chironomid head taxa.

Fig. S2: Broken-stick analysis based on square-root transformed percentages of non-rare chironomid taxa.

795 **Figures**

796 Fig 1

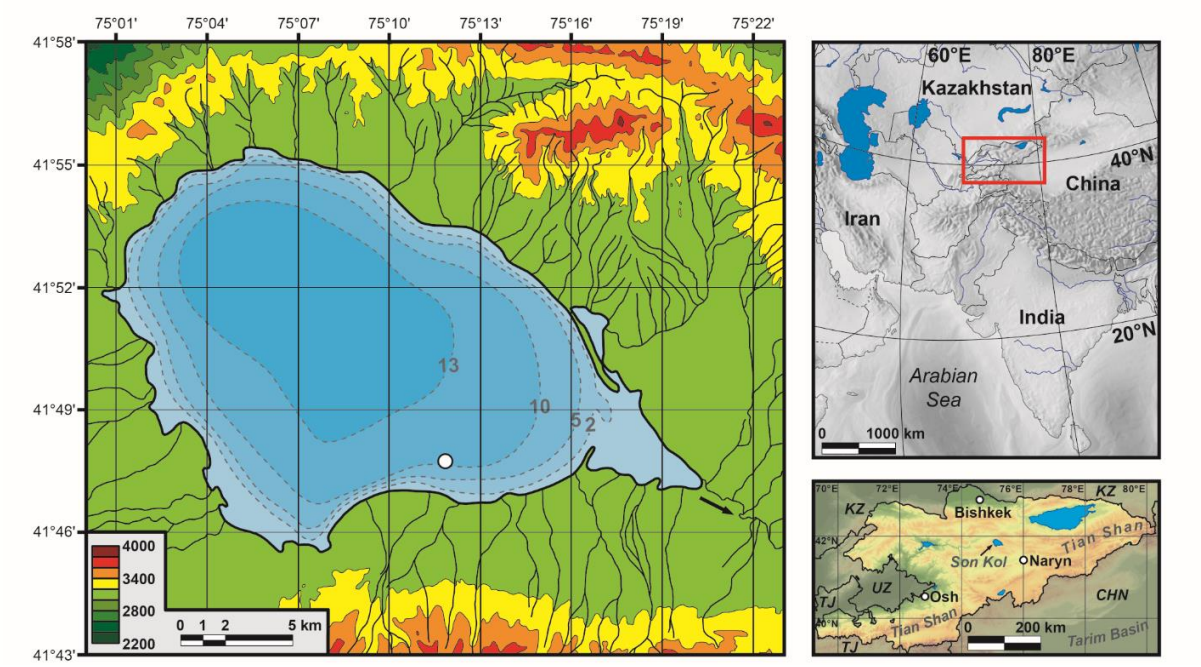

797

798

799 Fig 2

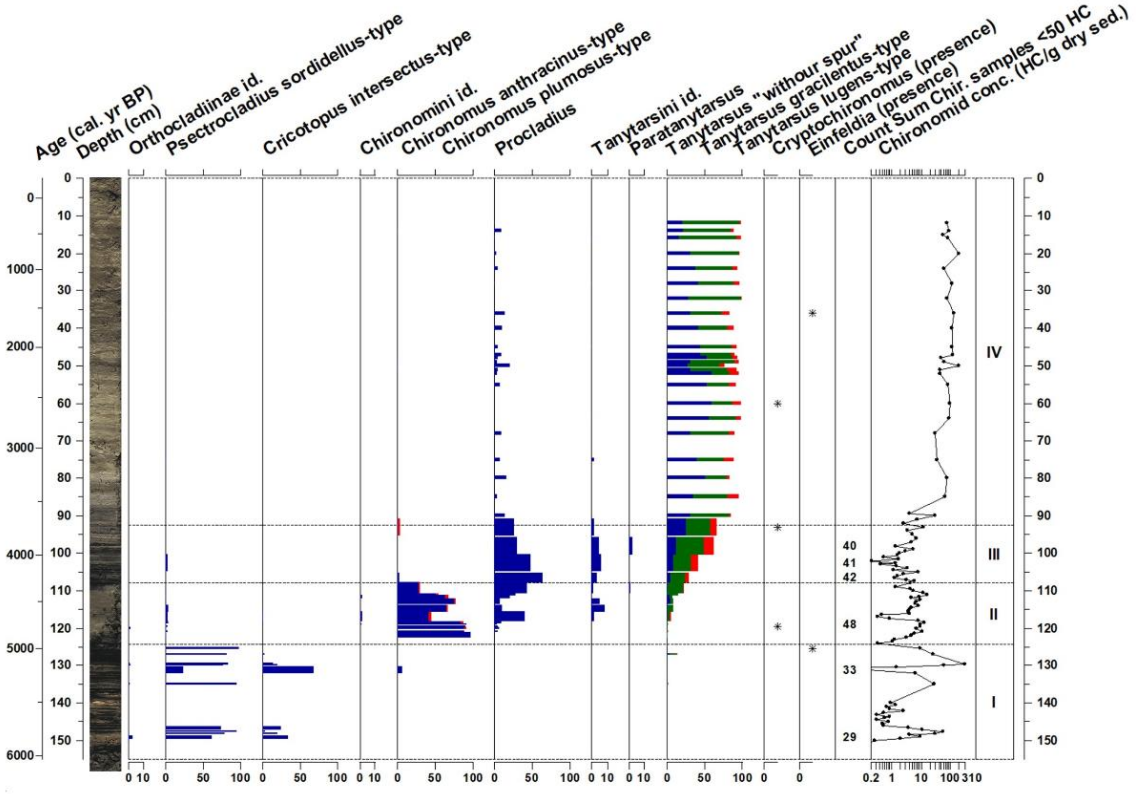

800

801

802 Fig 3

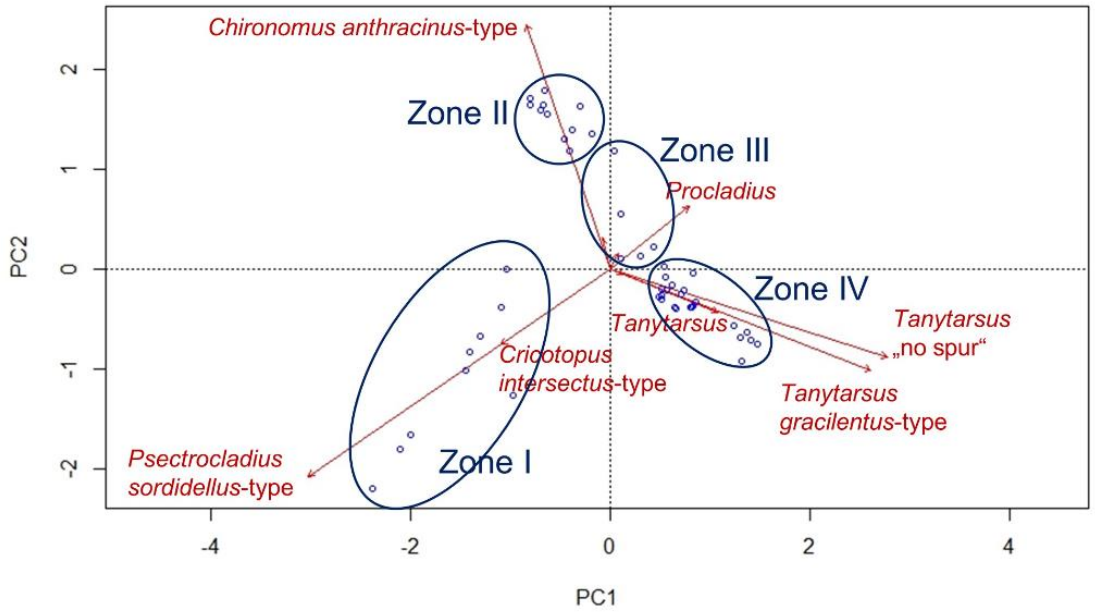

803

804

805 Fig 4

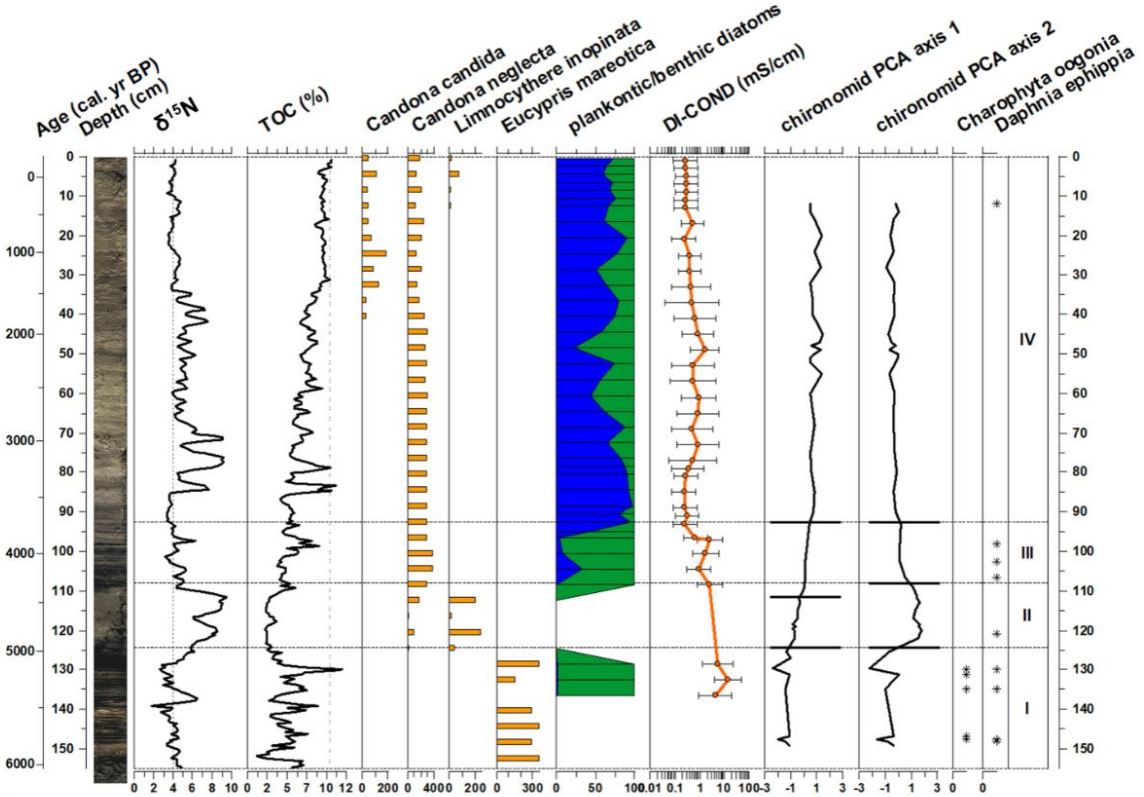

806

807

808 Fig 5

809

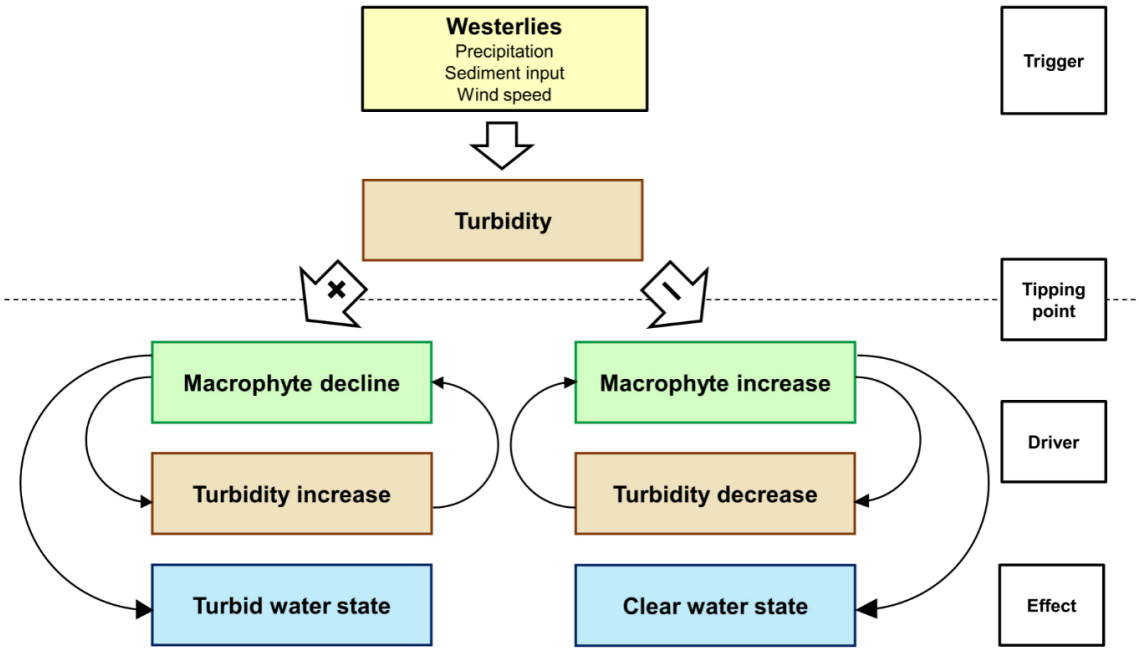
Westerlies
Precipitation
Sediment input
Wind speed
Trigger
Turbidity
Tipping point
Macrophyte decline
Macrophyte increase
Driver
Turbidity increase
Turbidity decrease
Turbid water state
Clear water state
Effect

810

811